European Journal of Medicinal Chemistry 224 (2021) 113737

Contents lists available at ScienceDirect

European Journal of Medicinal Chemistry

journal homepage: http://www.elsevier.com/locate/ejmech

Synthesis, structure-activity relationships and molecular docking studies of phenyldiazenyl sulfonamides as aromatase inhibitors

Letizia Giampietro [a, *], Marialucia Gallorini [b], Nicola Gambacorta [c], Alessandra Ammazzalorso [a], Barbara De Filippis [a], Alice Della Valle [a], Marialuigia Fantacuzzi [a], Cristina Maccallini [a], Adriano Mollica [a], Amelia Cataldi [b], Orazio Nicolotti [c], Rosa Amoroso [a]

[a] Unit of Medicinal Chemistry, Department of Pharmacy, "G. d'Annunzio" University, Chieti, Italy
[b] Unit of Anatomy, Department of Pharmacy, "G. d'Annunzio" University, Chieti, Italy
[c] Department of Pharmacy-Drug Science, University of Bari "Aldo Moro", Via E. Orabona, 4, 70126, Bari, Italy

ARTICLE INFO

Article history:
Received 17 May 2021
Received in revised form
29 July 2021
Accepted 1 August 2021
Available online 3 August 2021

Keywords:
Aromatase inhibitors
Breast cancer
Sulfonamide
Stilbene
Phenyldiazenyl
MCF7
Cell cycle
Apoptosis
CYP19A1
Docking simulations

ABSTRACT

The exploration of innovative aromatase inhibitors represents an important approach for the identification of new therapeutic treatments of breast cancer. In this respect, a series of phenyldiazenyl sulfonamides was designed, synthesized and tested. Compounds **3b**, **3f** and **5f** showed an aromatase inhibition in the micromolar range and were evaluated *in vitro* on the human breast cancer cell line MCF7 by MTT assay, cytotoxicity assay (LDH release), cell cycle analysis and apoptosis, revealing a dose-dependent inhibition profile. In particular, **3f** displayed the best reduction in terms of metabolic activity and an anti-proliferative effect on MCF7 cells, being blocked in the G1/S phase checkpoint. Moreover, computational studies were carried out to better understand at a molecular level of detail the rationale behind the effective binding to the active site of aromatase of the more active inhibitor **3f**. The obtained results allow to consider this compound as an interesting lead for the development of a new class of non-steroidal aromatase inhibitors.

1. Introduction

Aromatase cytochrome P450 (CYP) enzyme complex is responsible for estrogen biosynthesis. In particular, the steroidal sex hormone estrogens (estrone, 17β-estradiol) are biosynthesized by the conversion of their corresponding androgens, androstenedione and testosterone [1,2]. In this regard, the Cytochromes P450 (CYP450) are responsible for catalyzing the aromatization of the six-membered alicyclic moiety of these compounds to produce estrogen rings. These enzymes are highly expressed in men, but especially in the peripheral adipose tissue of postmenopausal women, in the ovaries of premenopausal women and in the placenta of pregnant women [3]. CYP450 enzymes carry a polypeptide chain comprising 503 amino acids including a Fe^{2+}-bearing heme moiety [4,5].

The androstenedione, whose chemical structure is shown in Fig. 1, is the natural substrate of aromatase being involved in the coordination of the Fe^{2+}-bearing heme group at the enzyme active site [5].

Its aromatization proceeds *via* three successive oxidation steps with the conversion of androgens (C19) to estrogens (C18) by demethylation and aromatization of the steroidal A-ring [6]. The gene of aromatase, CYP19, is located on chromosome 15q21.1 and codes cytochrome $P450_{arom}$. Estrogens are responsible for a variety of physiological functions in numerous tissues in both females and males. For examples, they exert physiological activity in reproductive/gonadal tissue, in neuroendocrine tissue, in adipose tissue and bone but they also play a pivotal role in the regulation of

* Corresponding author. Department of Pharmacy, University of Chieti "G. d. Annunzio", Via Dei Vestini, 31, 66100, Chieti, Italy.
E-mail address: letizia.giampietro@unich.it (L. Giampietro).

https://doi.org/10.1016/j.ejmech.2021.113737
0223-5234/

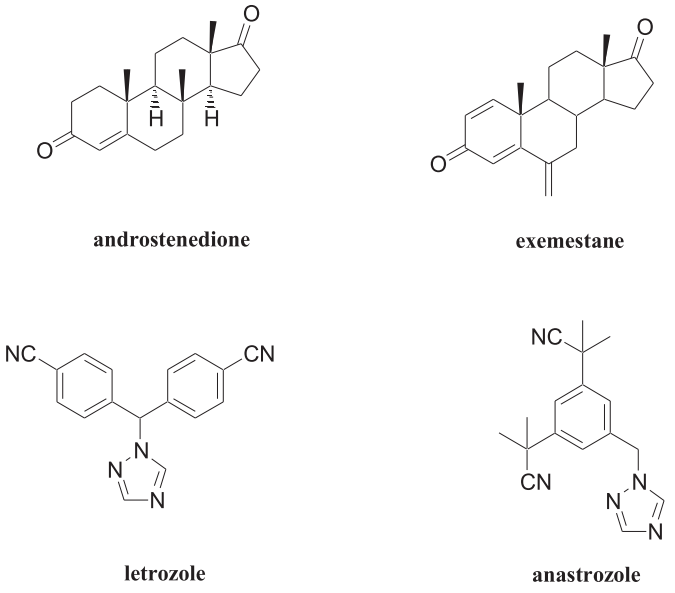

Fig. 1. Chemical structures of natural substrate of aromatase, steroidal and non-steroidal third generation of AIs.

calcium homeostasis with beneficial effects in preventing heart diseases, osteoporosis, and Alzheimer's disease [7].

Disorder of aromatase levels can initiate several pathological conditions in both genders [8]. In particular, postmenopausal estrogen-dependent breast cancer is the most common female cancer. In this case, an abnormally elevate expression of aromatase causes an increase of the production of estrogens with consequent growth and progression of the pathology [9]. Therefore, the inhibition of estrogen biosynthesis by aromatase inhibitors (AIs) constitutes one of the principal therapies for postmenopausal estrogen-dependent breast cancer [10].

The research on the development of the AIs began in the 1970s and has expanded significantly in recent years [11]. At first, competitive inhibitors were developed [12,13]; compounds as exemestane (Fig. 1) are defined as steroidal Ais. They bind irreversibly the catalytic site of aromatase P450 as well as the substrate androstenedione by determining a permanent inhibition of the enzyme. Non-steroidal AIs interfere reversibly with steroid hydroxylation by the binding with the heme iron of the CYP450. Aminoglutethimide was the first non-steroidal AI to be used although no longer in use for the occurrence of several side effects [14]. For these reasons, a lot of studies have been conducted to develop safer non-steroidal AIs.

The third generation of AIs, including drugs such as anastrozole and letrozole (Fig. 1), is clinically used and well tolerated; such inhibitors are more effective than tamoxifen in postmenopausal patients with metastatic breast cancer [15]. However, these AIs show side effects, such as increase of bone loss, joint pain, heart problems, and cellular resistance, especially after prolonged therapy with a potential acquired resistance [16,17].

For these reasons, during the last years, the discovery of new potent and selective molecules with lower side effects and devoid of resistant phenomena, has been a goal of utmost importance in medicinal chemistry programs focused on breast cancer research.

Natural compounds, such as stilbenes and stilbenoids, have been shown to have anti-inflammatory, cardioprotective, neuroprotective, antiobesity, antiangiogenic, antiproliferative and cancer chemopreventive effects [18,19] and they have also been shown to function as AIs [20]. In particular, resveratrol (Fig. 2) is one of the most studied natural compounds, although it is considered a poor drug candidate for its low potency, lack tissue and target specificity, rapid metabolism, and low serum concentrations [21]. For this reason, many stilbene analogues have been synthesized in order to improve the pharmacokinetic properties and to enhance the activity [18,22]. In particular, several resveratrol analogues have been developed with the aim to improve the anticancer activity [23] especially as AIs [20,24]. For example, Sun et al. synthesized different derivatives and among them, 4-aminostilbene (H-2-29) with an $IC_{50} = 22$ μM showed a better aromatase inhibition than resveratrol ($IC_{50} = 80$ μM) (Fig. 2) [25].

Through the use of classical bioisosterism in the stilbenoid nucleus, it is possible to obtain resveratrol analogues [26]. The phenyldiazenyl bioisostere of stilbene has been shown to be an important scaffold in medicinal chemistry. The C═C bond is a bridge between the two phenyl rings of stilbene that plays an important role especially in the antioxidant activity, allowing an electronic delocalization on the whole molecule [27]. Applying simple rules of bioisosterism, it is possible to replace the C═C bond with the isosteric N═N bond, obtaining azostilbene derivatives with interesting biological activities [28,29].

Sulfonamides have been shown to be an interesting option with a wide range of biological properties including anticancer, antimicrobial, antimalarial, and antiviral activities [30,31]. In particular, the sulfonamide pharmacophore is found in several AIs [32–35], and some of them are reported in Fig. 2. Through the oxygen and nitrogen atoms of the sulfonamide group these compounds could form hydrogen bonds with relevant residues of the target protein [36].

In the search for new non-steroidal AIs, we have recently discovered a series of sulfonamide derivatives [37–39]. In the present work, we report the synthesis, the biological evaluation, and the docking studies of a series of new sulfonamide compounds. To this end, we considered that stilbene is a scaffold present in many natural and synthetic compounds with aromatase inhibition and also anticancer chemopreventive effects [20]. In the current study, in order to investigate how the phenyldiazenyl bioisoster of stilbene and sulfonamide moieties can be combined in a single molecule with the aim to exploit their positive features as AIs, non-steroidal compounds containing these two pharmacophores were developed.

As shown in Fig. 3, we joined the phenyldiazenyl bioisoster of stilbene and sulfonamide moieties in a single molecule assuming that the integration of these two pharmacophore features could be effective for the rational design of new and more potent AIs.

The phenyldiazenyl moiety was kept unchanged and the sulfonamide group, which should be involved in making hydrogen bonds, was decorated with different aromatic or alkyl groups that should interact with the hydrophobic pocket of the enzyme. The sulfonamide nitrogen is not included in a cycle and, in some new compounds, it was substituted with a methylbenzimidazole group in order to investigate whether this pendant is able to interact with the heme iron or to generate van der Waals contacts.

The inhibition of human aromatase was measured as percentage of inhibition through an *in vitro* kinetic study by a fluorescence-based assay using letrozole as reference compound. The IC_{50} was then calculated for the compounds with the best activity. The cell viability and cytotoxicity were also evaluated by using MTT assay and LDH release assay over the MCF7 breast cancer cell line using resveratrol as reference compound. The apoptosis occurrence and the modulation of cell cycle were afterwards analyzed in the presence of the most promising compound. Further, a docking study was performed to evaluate how the best active compound approaches the active site of the enzyme.

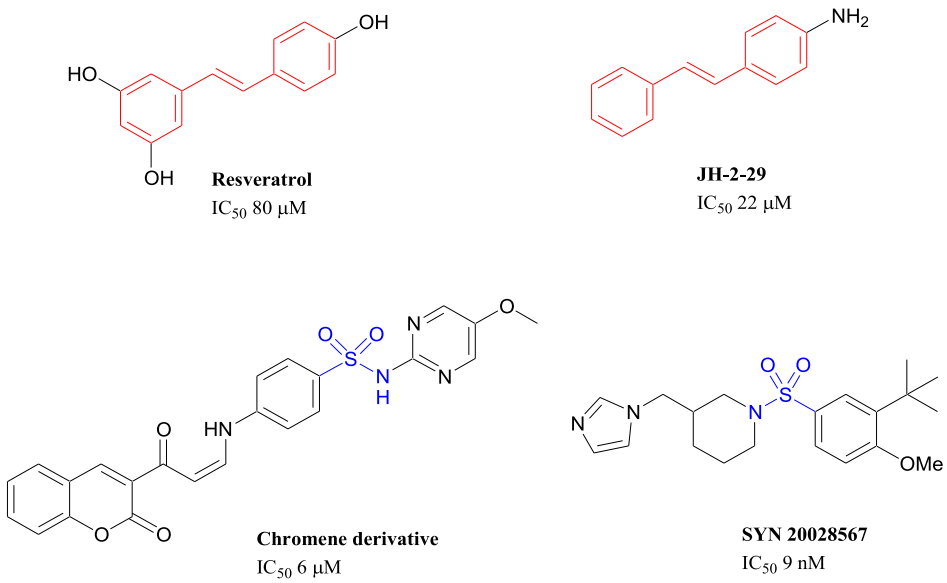

Fig. 2. Representative aromatase inhibitors containing stilbene and sulfonamide moieties.

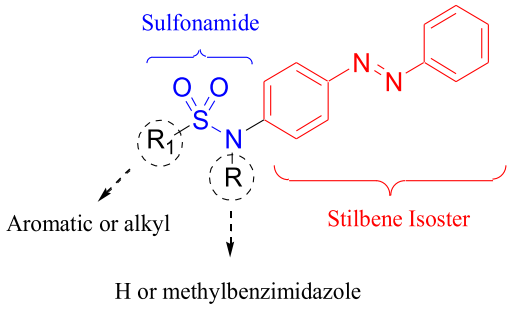

Fig. 3. Analogue-based design of new stilbene sulfonamide derivatives as AIs.

2. Results and discussion

2.1. Chemistry

The phenyldiazenyl sulfonamide compounds were synthesized as reported in Scheme 1. (*E*)-4-(phenyldiazenyl)aniline (**1**) was reacted with proper sulfonyl chloride (**2a-k**) to obtain (phenyldiazenyl)phenyl-benzenesulfonamides (**3a-k**).

In order to understand whether the introduction of a substituent in sulfonamide moiety improves the activity, we synthesized the benzoimidazol-methyl derivatives of compounds **3a**, **3c** and **3f** as depicted in Scheme 2. Compounds **3a**, **3c** or **3f** were reacted, at 0 °C and under N_2, with sodium hydride. The subsequent treatment with 2-(chloromethyl)benzimidazole (4) gave compounds **5a**, **5c** or **5f**.

2.2. In vitro aromatase inhibition assay

The human aromatase inhibitory activity of all synthesized compounds was determined using an *in vitro* fluorescence based assay (Aromatase CYP19A Inhibitor Screening Kit, BioVision). This assay employs a fluorogenic substrate that is converted into a highly fluorescent metabolite detected in the visible range (Ex/Em = 488/527 nm). Our compounds **3a-k** and **5a**, **5c**, **5f** were dissolved in acetonitrile and tested at 1 μM and compared with letrozole used as reference at the same concentration. The inhibition percentages were calculated with respect to letrozole with the 100% of aromatase inhibition. The percentages of inhibition of all new compounds are reported on Table 1.

Phenyldiazenyl sulfonamide compounds showed limited inhibition of aromatase with a percentage of inhibition lesser than 20% except for **3b**, **3f** and **5f**. Sulfonamide substitution in R_1 with 4-cyano-phenyl (**3b**) and with 2,4-dimethoxy-phenyl (**3f**) groups led to a strongly increase of the aromatase inhibition, when compared to letrozole, with values of 147% and 142%, respectively. The introduction of methyl-benzoimidazol substituent, instead of sulfonamide hydrogen of compound **3f**, led to a moderate inhibition of the enzyme for compound **5f** that showed a value of inhibition of 50%. However, this substitution resulted in a decrease of the activity referred to the unsubstituted analogue **3f**. For this reason, and because the other methyl-benzoimidazol derivatives **5a** and **5c** showed low percentage of aromatase enzyme inhibition (<20%), we decided to not synthesize the methyl-benzoimidazol analogues of compounds **3b**, **3d**, **3e** and **3g-k**.

After this first screening, compounds **3b**, **3f** and **5f**, which showed a percentage of aromatase inhibition greater than or equal to 50%, were selected to calculate the IC_{50}. Compounds were tested at five concentrations from 0.01 to 100 μM; the IC_{50} values were determined from the obtained concentration-response curves and reported in Table 2. In this table the IC_{50} value of resveratrol [27] is also reported because these compounds (**3b**, **3f** and **5f**) are its derivatives.

When benzensulfonamide was substituted in *para* position with a cyano group (**3b**), there was a strong increase of the activity compared to resveratrol. Compound **3b**, with an $IC_{50} = 7.9$ μM, was about ten times more active than resveratrol. Compound **3f** ($IC_{50} = 1.6$ μM) showed an increase of the activity five times more than **3b** and fifty times more than resveratrol. The *orto*/*para* dimethoxy substitution of the benzensulfonamide group returned the best activity for **3f** as AI. As expected, the introduction of the methyl-benzoimidazol group in compound **5f** ($IC_{50} = 5.7$ μM) implied a decrease of the activity if compared to **3f** but, however, 14-fold increase in activity if compared to resveratrol.

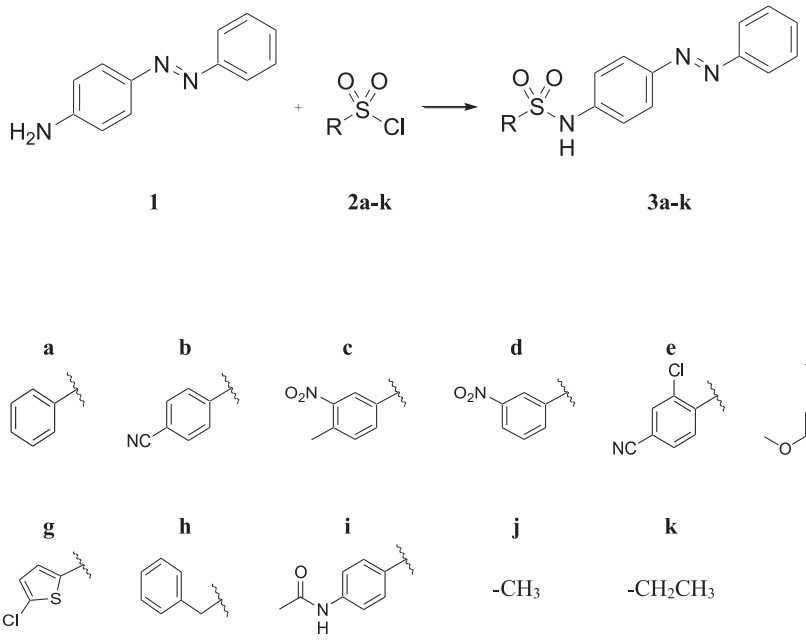

Scheme 1. Synthesis of compounds **3a-k**. Reagents and conditions: pyridine, DMF, 0–5 °C, r.t., 24h.

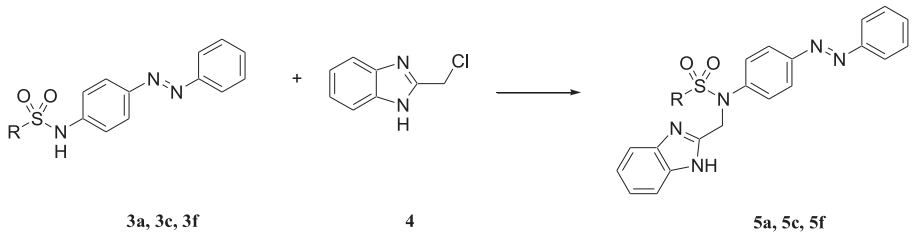

Scheme 2. Synthesis of compounds **5a**, **5c**, **5f**. Reagents and conditions: Sodium hydride 60% dispersion in mineral oil, DMF dry, 0–5 °C, N_2, r.t., 30′, r.t., 3–4 days.

2.3. In vitro evaluation of biological effects on human breast cancer cells (MCF7), cytotoxicity and selectivity against human fibroblasts (HFF-1)

Phenyldiazenyl sulfonamides **3b**, **3f** and **5f** can be considered resveratrol derivatives because the C=C bond of stilbene moiety was replaced with the isosteric N=N bond. As reported in literature, resveratrol has an IC_{50} of 80 μM on the aromatase enzyme [27]; replacing the C=C bond with N=N bond and introducing benzensulfonamide moiety, compounds **3b**, **3f** and **5f** with IC_{50} values of 7.9, 1.6 and 5.7 μM respectively, showed a good improvement of the inhibitory activity on aromatase when compared to resveratrol. For this reason, increasing concentrations (0–250 μM) of **3b**, **3f** and **5f** were administered up to 72 h to evaluate the biological effectiveness of the most promising compounds on the human breast cancer cell line MCF7 in terms of cell metabolic activity [MTT (3-(4,5-dimethylthiazol-2-yl)-2,5-diphenyltetrazolium bromide) test] and cytotoxicity [LDH (lactate dehydrogenase) assay]. The biological activity of the compounds was compared to that of resveratrol, here used as reference compound (Fig. 4 and Fig. 5A).

At the earliest exposure time (24 h), all the administered compounds reveal a weak but significant reduction (around 20%) in terms of cell metabolic activity with respect to resveratrol up to the 50 μM concentration, mainly in the presence of **3b** and **3f**. At higher concentrations, the **3f** displays the best reduction of cell metabolic activity (47.4% of metabolically active cells at 100 μM) compared to DMSO alone (100%) and resveratrol (78.2%). Interestingly, a dramatic peak in the LDH released from MCF7 cells is registered with **3f** at 50 μM after 24 h (2.5 folds more than DMSO alone), being besides the highest value registered for this set of experiments (Fig. 5A).

Indeed, a significant increase in the LDH leakage cannot be assessed for the other compounds, including resveratrol. This trend is maintained also at the highest administered concentration (250 μM). Based on these results, we can hypothesize that **3f** is cytotoxic for MCF7 cells showing the best reduction of cell metabolic activity and the highest value of LDH released.

A key signature for necrotic cells is the permeabilization of plasma membrane, observed both in normal and pathological diseases [40]. Since the release of LDH is enhanced in cells showing a damaged cell membrane because of late apoptosis and necrosis occurrence, the Annexin V-Propidium iodide assay was carried out at 24 h on MCF7 cells in the presence of the most cytotoxic compound 3f. In accordance with the LDH data, a significant dose-dependent increase of the percentage of cells found in the apoptotic stage is assessed in the presence of **3f** at 100 μM (19.7%) and at 250 μM (14.7%) compared to the control sample (7.3%). Likewise, percentages related to necrotic cells are higher with respect to the control, confirming the LDH data (Fig. 5B).

Furthermore, no significant differences between the three compounds can be registered after 48 h up to 50 μM as regards cell

Table 1
In vitro aromatase inhibition for compounds **3a-k** and **5a**, **5c** and **5f**.

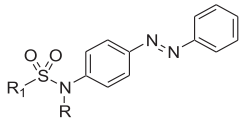

Compound	R	R_1	Percentage of aromatase enzyme inhibition
3a	H		<20%
5a	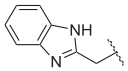		<20%
3b	H	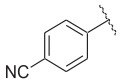	147%
3c	H	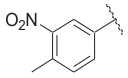	<20%
5c	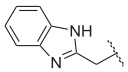		<20%
3d	H	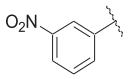	<20%
3e	H	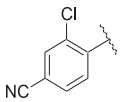	<20%
3f	H	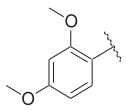	142%
5f	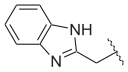		50%
3g	H	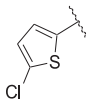	<20%
3h	H	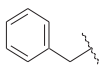	<20%
3i	H	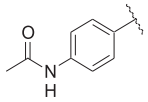	<20%
3j	H	-CH_3	<20%
3k	H	-CH_2CH_3	<20%
Letrozole			100%

Table 2
The IC_{50} values of the aromatase-active compounds **3b**, **3f** and **5f**.

Compound	IC_{50} values of the aromatase (μM)
3b 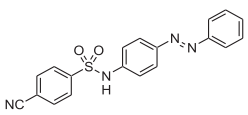	7.9
3f 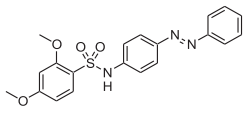	1.6
5f 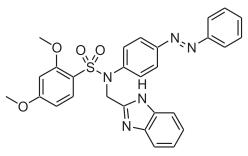	5.7
Resveratrol	80

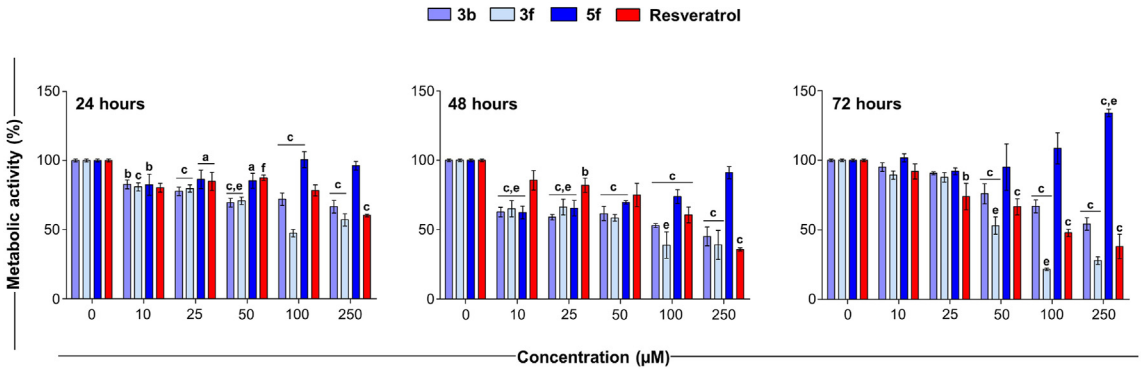

Fig. 4. Cell metabolic activity of human breast cancer cells (MCF7) in the presence of increasing concentrations of compounds **3b**, **3f** and **5f** after 24, 48 and 72 h. Data shown are the means ± standard deviations of three replicates (n = 9) and are expressed as percentages of cultures in the presence of vehicle (DMSO) set as 100%. a = $p < 0.01$; b = $p < 0.001$; c = $p < 0.0001$ between compounds and DMSO; e = $p < 0.001$; f = $p < 0.0001$ between compounds and resveratrol at the same concentration.

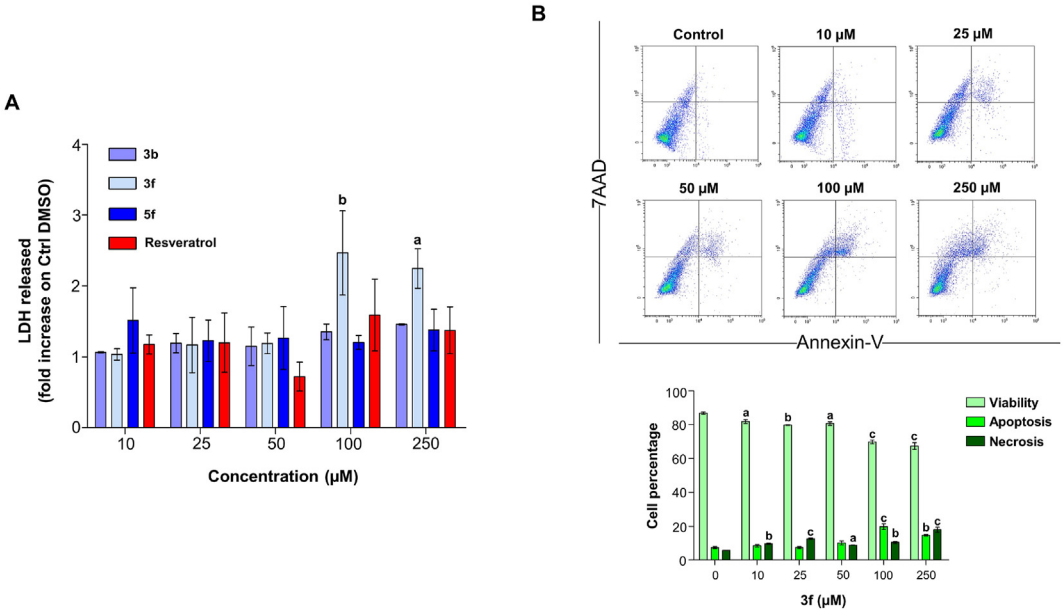

Fig. 5. Cytotoxicity and apoptosis occurrence in human breast cancer cells (MCF7) after 24 h. (A) Lactate dehydrogenase released (LDH) in the presence of increasing concentrations of compounds **3b**, **3f** and **5f**. Data shown are the means ± standard deviations of three replicates (n = 9) and are expressed as the fold increase on the LDH released by cultures in the presence of vehicle (DMSO) set as 1 (not shown). (B) Dot plots are representative images showing the distribution of the cell population in the various phases of apoptosis and necrosis: viable cells (lower left quadrant), early apoptotic cells (lower right quadrant), late apoptotic cells (upper right quadrant) and necrotic cells (upper left quadrant). The bar graph summarizes the percentage of viable cells (Annexin-V and 7AAD negative), cells in apoptosis (Annexin-V and 7AAD positive) and cells in necrosis (7AAD positive) as means ± S.D. of three replicates (n = 3).
a = $p < 0.01$; b = $p < 0.001$; c = $p < 0.0001$ between compounds and DMSO.

metabolic activity. Compared to the 24 h administration, metabolically active cells in the presence of all the compounds are fewer, being percentages of metabolic activity around 60%. Once again, **3f** displays the best reduction in terms of metabolic activity with respect to both DMSO alone and resveratrol. Finally, when compounds are administered for 72 h on MCF7 cells, a dose-dependent decrease of cell metabolic activity can be registered for compounds **3b**, **3f** and resveratrol, definitively showing that **3f** is the best compound in decreasing the percentage of metabolically active cells.

For the sake of completeness, the cell cycle profile of MCF7 cells in the presence of increasing concentrations of the most promising compound **3f** was evaluated. It has been frequently reported that aromatase inhibitors are able to induce a decrease in cell proliferation, and these anti-proliferative effects seem to be due to a disruption in cell cycle progression and cell death enhanced through the apoptosis induction [41]. In our experimental model, the decrease of cell metabolic activity at 72 h is confirmed by the analysis of cell cycle at the same experimental time in the presence of **3f**, which highlights a dose-dependent reduction of cells found in the S phase and an increase of the G1 phase at the highest concentrations administered (Fig. 6).

In the mammary gland, estrogens promote cell proliferation acting as mitogens and can modify the expression of hormone-responsive genes involved in the progression of cell cycle and/or programmed cell death through activation of estrogen receptors (ERs). It has been reported that estradiol stimulates MCF7 proliferation and growth through the induction of the G1/S phase transition and protects toward apoptosis, whereas estrogens deprivation through aromatase inhibitors inhibits cell proliferation and induces apoptosis in breast cancer models [41]. Based on our results, it is plausible to assume that our potent aromatase inhibitor

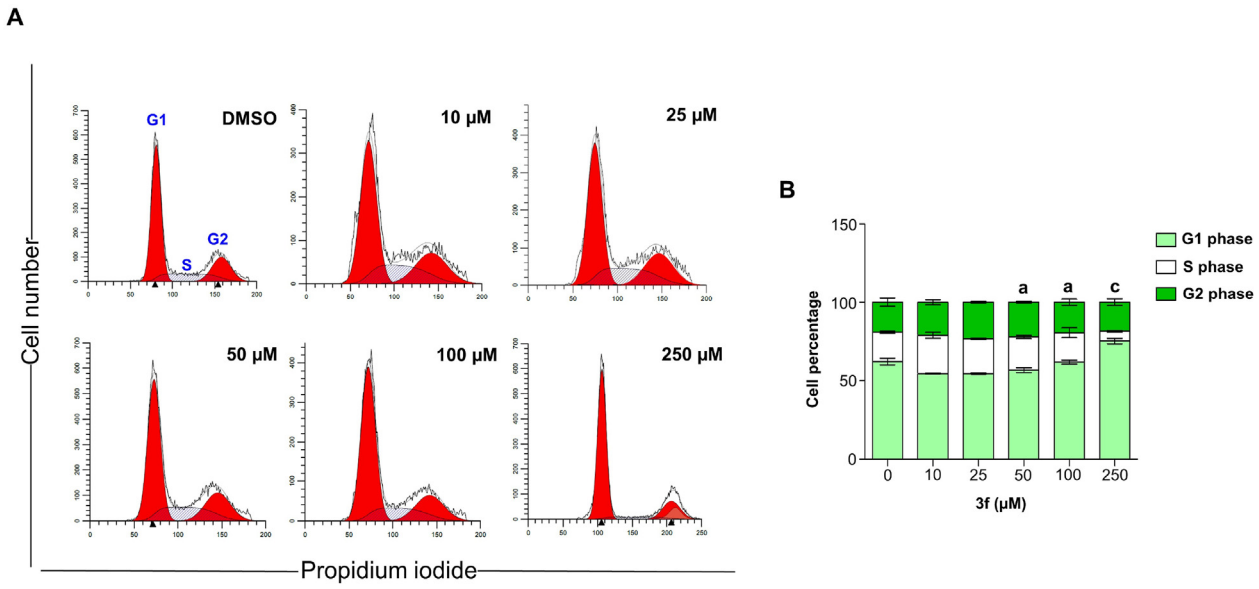

Fig. 6. Cell cycle analysis in the presence of increasing concentrations of compound **3f** in MCF7 cells after 72 h. (A) Cell cycle profiles represented by fluorescence emission peaks obtained after the propidium iodide staining (y-axis = cell count; x-axis = propidium iodide fluorescence emission in the FL-3 channel). (B) The bar graph shows cell percentages in the various phases of cell cycle (G1, S, and G2). Data are reported as means ± standard deviations of independent experiments (n = 3).
a = $p < 0.01$; b = $p < 0.001$; c = $p < 0.0001$ between compounds and DMSO.

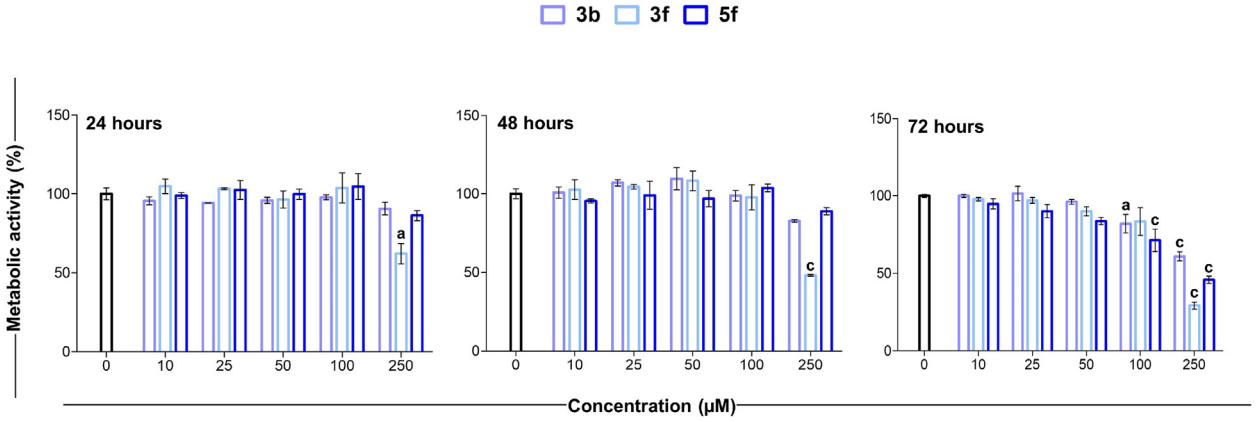

Fig. 7. Cell metabolic activity of human fibroblasts (HFF-1) in the presence of increasing concentrations of compounds **3b**, **3f** and **5f** after 24, 48 and 72 h. Data shown are the means ± standard deviations of three replicates (n = 3) and are expressed as percentages of cultures in the presence of vehicle (DMSO) set as 100%. a = $p < 0.01$; b = $p < 0.001$; c = $p < 0.0001$ between compounds and DMSO.

3f behaved similarly, thus acting as an anti-proliferative agent on MCF7 cells, which are blocked in the G1/S phase checkpoint.

As a whole, **3f** is supposed to exert the best performance on breast cancer cells having the lowest IC_{50} registered on the aromatase enzyme (1.6 μM) compared to **3b** (7.9 μM) and resveratrol (80 μM). Contrariwise, compound **5f** behaves differentially; in detail, it shows a weak reduction of cell metabolic activity percentages up to 50 μM comparable to the other two compounds and to resveratrol. Moreover, MCF7 cells seem to recover and this effect is dose and time-dependent, being the percentage of metabolically active cells assessed at 134.2% at 250 μM after 72 h. However, compound **5f** seems to bind the aromatase enzyme better than **3b**, being the IC_{50} assessed at 5.7 μM. As described for other aromatase inhibitors tested on the MCF7 cell line, this behavior could be ascribed to mechanisms related to chemoresistance [39–43].

Being aware that (ER)-positive breast cancer cells can adapt to estrogen deprivation during aromatase inhibitors treatment (i.e., letrozole) by activating alternative signaling pathways [44], and that MCF7 LTED (Long-Term Estrogen Deprived) show a higher amount of exosomal RNA delivering information to promote metastasis and drug resistance with respect to MCF7 cells [45], a similar behavior is likely to be adopted by **3f**. Nevertheless, deeper molecular studies on **3f** will clear up the biological actions related to the observed promising effects.

In order to evaluate the selectivity against a non-cancerous cell line, compounds **3b**, **3f** and **5f** were also tested on the normal human fibroblast cells (HFF-1) [46]. Also in this case, increasing concentrations (0–250 μM) of **3b**, **3f** and **5f** were administered up to 72 h and cell metabolic activity through the MTT was evaluated (Fig. 7).

All the tested compounds are not effective on HFF-1 cells and a reduction of cell metabolic activity can be registered only at the highest concentration administered (250 μM), especially for compound **3f**. The selectively index (SI) was calculated as follows: SI =

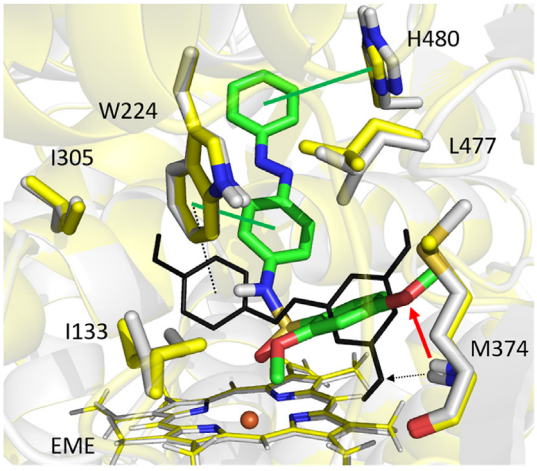

Fig. 8. Zoomed in view at aromatase CYP19A1 binding site. Two conformations of receptor returned from induced-fit docking are shown with yellow and white cartoon, for **3f** and resveratrol, respectively. Compound **3f** and resveratrol are rendered as green sticks and black wireframes, respectively. Eme group and Fe^{2+} ion are rendered as white wireframes and orange sphere, respectively. Hydrogen bonds are depicted with red and black dashed arrows, and π-π contacts are depicted with and green and black dashed lines, for **3f** and resveratrol, respectively.

IC_{50} on normal fibroblast cells (HFF-1)/IC_{50} on cancer cell line (MCF7). Compounds **3b** and **5f** show some selectivity only at 24 h (**3b** SI > 1.6; **5f** SI > 2.55). Nevertheless, compound **3f** displays an increase of the selectivity index from 24 h to 72 h. In particular, this molecule shows a SI = 2.12 after 24 h, a SI = 3.19 after 48 h and a SI = 3.74 after 72 h. These results corroborate the hypothesis that 2,4-dimethoxy-phenyldiazenyl-phenyl-benzenesulfonamide derivative (**3f**) is the most promising AI with a powerful decrease of MCF7 viability and a notable SI towards HFF-1, which is more consistent after longer exposure.

2.4. Computational studies

To help the interpretation of biological data and to increase our understanding of the molecular bases for the more active aromatase inhibitor **3f** referred to resveratrol, we carried out some computational simulations in order to study the molecular interactions responsible for the effective binding to the active site of aromatase.

Molecular interactions engaged by compound **3f** and resveratrol to target aromatase CYP19A1 were investigated by performing induced-fit docking simulations and MM-GBSA calculations. In this respect, the computed values for docking score were equal to −9.111 kcal/mol and −9.577 kcal/mol, and MM-GBSA free energies were equal to −76.15 kcal/mol and −26.47 kcal/mol, for **3f** and resveratrol, respectively.

Looking at Fig. 8, compound **3f** can engage π-π interactions through its azobenzene moiety with H480 and W224, the latter already flagged in a previous work concerning resveratrol based aromatase inhibitors [25]. Furthermore, the *para*-methoxy group can establish a hydrogen bond with the nitrogen of M374 backbone. Noteworthy, this interaction is also experienced by the X-ray solved carbonyl group of androstenedione cognate ligand in complex with CYP19A1 aromatase and by the hydroxyl group of resveratrol. Overall, a network of hydrophobic interactions made with I133, W224, I305, M374, L477 and H480 side chains contributes significantly to ligand binding.

Computational studies have been employed in order to shed light on the interactions of **3f** towards CYP19A1 aromatase and have given a sound explanation at molecular level of experimental data. Although resveratrol returned a slightly better docking score value than that of **3f**, a substantial gap concerning the MM-GBSA value in favor of the latter was observed. MM-GBSA method performs a rescoring of selected docking poses and exploits empirical corrections for describing hydrogen bonds and hydrophobic interaction [47], thus returning more reliable results, which are in agreement with the experimental data.

As far as the binding mode is concerned, compound **3f** can explore a wider area of the binding pocket compared to that visited by resveratrol, impacting with an additional hydrophobic area made up by L477 and H480. Interestingly, the induced-fit docking protocol allows to introduce structural changes in the receptor. Therefore, it can suggest which residue in the binding pocket can slightly shift its conformation to better accommodate **3f**. In particular, hydrophobic side chains of L477 and H480 slightly move their positions to give access to the azobenzene moiety of **3f**, as well as I133 with respect to its benzosulfonamide moiety.

3. Conclusion

A series of sulfonamides with phenyldiazenyl bioisoster of stilbene moiety was synthesized and evaluated as aromatase inhibitors by an *in vitro* enzymatic assay. Three compounds, **3a**, **3f** and **5f** showed a percentage of enzymatic inhibition better than letrozole and IC_{50} values, in the range of micromolar (7.9, 1.6 and 5.7 μM, respectively), 10 to 50 times better than IC_{50} of resveratrol (80 μM). These three compounds were evaluated *in vitro* on MCF7 breast cancer cells by MTT assay and cytotoxicity assay. The best results were obtained for compound **3f** and were confirmed by the analysis of cell cycle and apoptosis. A significant dose-dependent increase of the percentage of cells found in the apoptotic stage was assessed in the presence of **3f**; moreover, **3f** showed an anti-proliferative effect on MCF7 cells, being blocked in the G1/S phase checkpoint. Furthermore, **3f** was also not effective on HFF-1 showing an increase of the selectivity index from 24 h to 72 h.

Computational studies were carried out and gave a sound explanation at molecular level of experimental data. The obtained results allow to consider **3f** as an interesting lead for the development of a new class of non-steroidal aromatase inhibitors.

4. Experimental section

4.1. Chemistry

Büchi B-540 apparatus was used to measure melting points and these values were uncorrected. Infrared spectra were recorded on a FT-IR 1600 Perkin−Elmer spectrometer. A Varian instrument was utilized to run NMR spectra at 300 MHz using tetramethylsilane as an internal reference, and chemical shifts (δ) are reported in ppm. Splitting patterns are designed as s, singlet; d, doublet; t, triplet; q, quartet; dd, double doublet; m, multiplet; b, broad.

Elemental analyses were carried out using a PerkinElmer 240 B microanalyzer and were found to be within ±0.4% of the theoretical values for C, H, and N for all compounds. The purity of all compounds was over 98%. All commercial and cell culture reagents, medium and reference compounds were obtained from Sigma-Aldrich (Milan, Italy). Chemical reactions were monitored by thin-layer chromatography (TLC) on F254 silica gel 60 TLC plates. Flash chromatography was performed on silica gel 60 (Merck).

4.1.1. General procedure for synthesis of compounds ***3a-k***

To a solution of (*E*)-4-(phenyldiazenyl)aniline (**1**) (0.507 mmol, 0.1000 g) in DMF (0.400 mL/mmol) at 0 °C was added slowly pyridine (0.400 mL/mmol) and proper sulfonyl chloride (**2a-k**)

(0.507 mmol). The reaction was allowed to stir at room temperature for 24 h. After completion of the reaction, the resulting mixture was poured into water (10 mL) and extracted with ethyl acetate (3 × 10 mL). The combined organic layers were washed with water (30 mL), brine (30 mL), dried over Na_2SO_4, filtered and concentrated under reduced pressure. Purification by column chromatography on silica gel (CH_2Cl_2 100% or cicloexane:AcOEt 9:1) gave compounds **3a-k**.

4.1.1.1. (E)-N-(4-(phenyldiazenyl)phenyl)benzenesulfonamide ***3a***. Orange solid, yield 60%; m.p. 137–138 °C; IR (KBr) 3268, 1328, 1158 cm^{-1}; ^1H NMR ($CDCl_3$) δ 6.84 (s, 1H, N*H*), 7.22 (d, 2H, *H*arom), 7.44–7.55 (m, 6H, *H*arom), 7.81–7.88 (m, 6H, *H*arom); ^{13}C NMR ($CDCl_3$) δ 120.21, 122.79, 124.20, 127.24, 129.10, 129.25, 131.04, 133.39, 138.74, 138.82, 149.67, 152.49. Anal. calcd for $C_{18}H_{15}N_3O_2S$: C 64.08, H 4.48, N 12.45; Found C 64.15, H 4.46, N 12.48.

4.1.1.2. (E)-4-cyano-N-(4-(phenyldiazenyl)phenyl)benzenesulfonamide ***3b***. Orange solid, yield 65%; m.p. 179–180 °C; IR (KBr) 3211, 2234, 1347, 1166 cm^{-1}; ^1H NMR ($CDCl_3$) δ 6.98 (s, 1H, N*H*), 7.23 (d, 2H, *H*arom), 7.48–7.53 (m, 3H, *H*arom), 7.76 (d, 2H, *H*arom), 7.84–7.94 (m, 6H, *H*arom); ^{13}C NMR ($CDCl_3$) δ 117.06, 121.61, 122.87, 124.36, 127.85, 129.16, 131.31, 133.04, 137.59, 137.64, 142.89, 150.23, 152.40. Anal. calcd for $C_{19}H_{14}N_4O_2S$: C 62.97, H 3.89, N 15.46; Found C 63.01, H 3.90, N 15.44.

4.1.1.3. (E)-4-methyl-3-nitro-N-(4-(phenyldiazenyl)phenyl)benzenesulfonamide ***3c***. Orange solid, yield 60%; m.p. 135–136 °C; IR (KBr) 3231, 1344, 1160 cm^{-1}; ^1H NMR ($CDCl_3$) δ 2.64 (s, 3H, C*H*$_3$), 7.00 (s, 1H, N*H*), 7.25 (d, 2H, *H*arom), 7.44–7.51 (m, 4H, *H*arom), 7.84–7.89 (m, 5H, *H*arom), 8.47 (d, 1H, *H*arom); ^{13}C NMR ($CDCl_3$) δ 20.66, 121.29, 122.85, 123.79, 124.37, 129.95, 129.13, 130.92, 131.22, 134.00, 137.83, 138.16, 139.31, 150.10, 152.44. Anal. calcd for $C_{19}H_{16}N_4O_4S$: C 57.57, H 4.07, N 14.13; Found C 57.50, H 4.08, N 14.10.

4.1.1.4. (E)-3-nitro-N-(4-(phenyldiazenyl)phenyl)benzenesulfonamide ***3d***. Gold solid, yield 63%; m.p. 180–182 °C; IR (KBr) 3277, 1348, 1166 cm^{-1}; ^1H NMR ($CDCl_3$) δ 7.00 (s, 1H, N*H*), 7.26 (d, 2H, *H*arom), 7.49–7.53 (m, 3H, *H*arom), 7.68 (t, 1H, *H*arom, J = 8.1 Hz), 8.84–7.88 (m, 4H, Harom), 8.11 (d, 1H, *H*arom) 8.42 (d, 1H, *H*arom, J = 8.1 Hz), 8.73 (s, 1H, *H*arom, J = 8.1 Hz); ^{13}C NMR ($CDCl_3$) δ 121.46, 122.49, 122.88, 124.40, 127.80, 129.15, 130.64, 131.30, 132.76, 137.60, 140.88, 150.20, 152.40, 155.99, 180.56. Anal. calcd for $C_{18}H_{14}N_4O_4S$: C 56.54, H 3.69, N 14.65; Found C 56.55, H 3.69, N 14.66.

4.1.1.5. (E)-2-chloro-4-cyano-N-(4-(phenyldiazenyl)phenyl)benzenesulfonamide ***3e***. Orange solid, yield 66%; m.p. 184–185 °C; IR (KBr) 3266, 2235, 1387, 1158 cm^{-1}; ^1H NMR ($CDCl_3$) δ 7.24–7.27 (m, 3H, *H*arom + N*H*), 7.48–7.53 (m, 3H, *H*arom), 7.65 (d, 1H, *H*arom), 7.80–7.87 (m, 5H, *H*arom), 8.18 (d, 1H, *H*arom); ^{13}C NMR ($CDCl_3$) δ 115.78, 118.19, 121.43, 122.86, 124.29, 129.13, 130.85, 131.31, 132.47, 132.73, 134.76, 137.00, 140.31, 150.35, 152.40. Anal. calcd for $C_{19}H_{13}ClN_4O_2S$: C 57.50, H 3.30, N 14.12; Found C 57.49, H 3.31, N 14.11.

4.1.1.6. (E)-2,4-dimethoxy-N-(4-(phenyldiazenyl)phenyl)benzenesulfonamide ***3f***. Orange solid, yield 61%; m.p. 176–177 °C; IR (KBr) 3232, 1317, 1149 cm^{-1}; ^1H NMR ($CDCl_3$) δ 3.79 (s, 3H, OC*H*$_3$), 3.99 (s, 3H, OC*H*$_3$), 6.43–6.84 (m, 2H, *H*arom), 7.22 (d, 2H, *H*arom), 7.44–7.49 (m, 3H, *H*arom), 7.60 (s, 1H, N*H*), 7.77 (d, 2H, *H*arom), 7.82–7.86 (m, 3H, *H*arom); ^{13}C NMR ($CDCl_3$) δ 55.69, 56.37, 99.43, 104.52, 117.96, 120.21, 122.71, 124.05, 129.08, 130.92, 133.01, 139.63, 149.35, 152.50, 157.69, 165.27. Anal. calcd for $C_{20}H_{19}N_3O_4S$: C 60.44, H 4.82, N 10.57; Found C 60.49, H 4.80, N 10.56.

4.1.1.7. (E)-5-chloro-N-(4-(phenyldiazenyl)phenyl)thiophene-2-sulfonamide ***3g***. Red solid, yield 64%, m.p. 135–137 °C; IR (KBr) 3230, 1318, 1147 cm^{-1}; ^1H NMR ($CDCl_3$) δ 6.86 (d, 1H, *H*thiop), 6.99 (s, 1H, N*H*), 7.29 (d, 2H, *H*arom), 7.36 (d, 1H, *H*thiop), 7.48–7.53 (m, 3H, *H*arom), 7.89 (d, 4H, *H*arom); ^{13}C NMR δ 121.30, 122.86, 124.29, 126.84, 129.13, 131.19, 132.69, 136.88, 138.04, 138.37, 150.14, 152.49. Anal. calcd for $C_{16}H_{12}ClN_3O_2S_2$: C 50.86, H 3.20, N 11.12; Found C 50.89, H 3.19, N 11.13;

4.1.1.8. (E)-1-phenyl-N-(4-(phenyldiazenyl)phenyl)methanesulfonamide ***3h***. Orange solid, yield 60%; m.p. 187–190 °C; IR (KBr) 3235, 1315, 1152 cm^{-1}; 1H NMR (CDCl3) δ 4.41 (s, 2H, CH2), 6.52 (s, 1H, NH), 7.23–7.35 (m, 4H, Harom), 7.35–7.39 (m, 3H, Harom), 7.48–7.55 (m, 3H, Harom), 7.90–7.95 (m, 4H, Harom); 13C NMR (CDCl3) δ 57.76, 119.21, 122.81, 124.52, 128.26, 128.99, 129.13, 130.82, 131.05, 139.36, 140.70, 149.34, 152.55. Anal. calcd for $C_{19}H_{17}N_3O_2S$: C 64.94, H 4.88, N 11.96; Found C 64.99, H 4.87, N 11.94.

4.1.1.9. (E)-N-(4-(N-(4-(phenyldiazenyl)phenyl)sulfamoyl)phenyl) acetamide ***3i***. Red solid, yield 58%; m.p. 157–161 °C; IR (KBr) 3238, 1311, 1148 cm^{-1}; ^1H NMR ($CDCl_3$) δ 2.19 (s, 3H, C*H*$_3$CO), 7.79–7.56 (m, 5H, Harom), 7.74 (d, 2H, Harom), 7.92–7.99 (m, 6H, Harom); ^{13}C NMR δ 29.6, 119.30, 122.00, 122.35, 125.35, 128.58, 129.30, 124.52, 135.50, 141.83, 145.72, 152.20, 168.40. Anal. calcd for $C_{20}H_{18}N_4O_3S$: C 60.90, H 4.60, N 14.20; Found C 60.91, H 4.59, N 14.21.

4.1.1.10. (E)-N-(4-(phenyldiazenyl)phenyl)methanesulfonamide ***3j***. Orange solid, yield 59%; m.p. 187–190 °C; IR (KBr) 3235, 1315, 1152 cm^{-1}; ^1H NMR ($CDCl_3$) δ 3.10 (s, 3H, C*H*$_3$), 6.66 (s, 1H, N*H*), 7.34 (d, 2H, *H*arom), 7.47–7.54 (m, 3H, *H*arom), 7.89–7.91 (m, 2H, *H*arom), 7.95 (d, 2H, *H*arom); ^{13}C NMR ($CDCl_3$) δ 39.84, 114.99, 119.75, 122.83, 124.57, 129.13, 131.09, 145.94, 152.52. Anal. calcd for $C_{13}H_{13}N_3O_2S$: C 56.71, H 4.76, N 15.26; Found C 56.73, H 4.5, N 5.28.

4.1.1.11. (E)-N-(4-(phenyldiazenyl)phenyl)ethanesulfonamide ***3k***. Orange solid, yield 57%, m.p. 164–166 °C; IR (KBr) 3230, 1318, 1149 cm^{-1}; ^1H NMR ($CDCl_3$) δ 1.41 (t, 3H, C*H*$_3$CH$_2$), 3.14 (q, 2H, CH$_3$C*H*$_2$), 7.36–7.55 (m, 6H, *H*arom + NH), 7.89–7.95 (m, 4H, *H*arom); ^{13}C NMR ($CDCl_3$) δ 8.27, 46.34, 119.47, 122.83, 124.55, 129.15, 131.05, 139.44, 149.41, 152.52. Anal. calcd for $C_{14}H_{15}N_3O_2S$: C 58.11, H 5.23, N 14.52; Found C 58.15, H 5.4, N 14.50.

4.1.2. General procedure for synthesis of compounds ***5a, 5c*** *and* ***5f***

To a solution of compound **3a**, **3c** or **3f** (1.2 eq) in DMF (9 mL/mmol) at 0 °C, under N_2, was added sodium hydride 60% dispersion in mineral oil (3 eq). The reaction was allowed to stir at room temperature for 30 min. After this period, the mixture was cooled at 0 °C and 2-(chloromethyl)benzimidazole (**4**) (1 eq) was added. After 2–4 days, the resulting mixture was poured into water (15 mL) and extracted with ethyl ether (3 × 15 mL). The combined organic layers were washed brine (3 × 15 mL), dried over Na_2SO_4, filtered and concentrated under reduced pressure. Purification by column chromatography on silica gel (CH_2Cl_2 100% or cicloexane:AcOEt 9:1) gave compound **5a**, **5c** or **5f**.

4.1.2.1. (E)-N-((1H-benzo[d]imidazole-2-yl)methyl)-N-(4-(phenyldiazenyl)phenyl)benzenesulfonamide ***5a***. Orange solid, yield 20%; m.p. 180–182 °C; IR (KBr) 3200, 1318, 1154 cm^{-1}; ^1H NMR ($CDCl_3$) δ 5.16 (s, 2H, C*H*$_2$), 7.22–7.29 (m, 3H, *H*arom), 7.48–7.60 (m, 9H, *H*arom), 7.66–7.70 (m, 3H, *H*arom), 7.76 (d, 2H, *H*arom), 7.85–7.88 (m, 2H, *H*arom); ($CDCl_3$) δ 49.56, 112.30, 114.79, 120.36, 121.47, 122.86, 123.67, 126.84, 128.75, 129.08, 131.21, 138.59, 140.90, 146.27, 149.17, 150.75, 156.29, 159.45. Anal. calcd for $C_{26}H_{21}N_5O_2S$: C 66.79, H 4.53, N 14.98; Found C 66.81, H 4.54, N 14.96.

4.1.2.2. (E)-N-((1H-benzo[d]imidazole-2-yl)methyl)-4-methyl-3-nitro-N-(4-(phenyldiazenyl)phenyl)benzenesulfonamide 5c. Red sticky solid, yield 30%; m.p. 187–188 °C; IR (KBr) 3210, 1320, 1150 cm^{-1}; ^1H NMR (Acetone-d6) δ 2.64 (s, 3H, CH_3), 5.32 (s, 2H, CH_2NSO_2), 7.26 (d, 1H, $CHCCH_3$), 7.43–7.54 (m, 5H, *CH*ar), 7.85 (d, 1H, $CHCSO_2$), 7.86–7.90 (m, 4H, *H*ar), 8.47 (s, 1H, $CHCNO_2$). ^{13}C NMR ($CDCl_3$): δ 20.66, 46.83, 115.20, 121.29, 122.85, 123.05, 124.37, 131.22, 134.00, 137.83, 138.16, 138.90, 139.31, 141.50, 149.10, 150.12, 158.35, 160.89, 161.36. Anal. calcd for $C_{27}H_{22}N_6O_4S$: C 61.59, H 4.21, N 15.96; Found C 61.57, H 4.22, N 15.93.

4.1.2.3. (E)-N-((1H-benzo[d]imidazole-2-yl)methyl)-2,4-dimethoxy-N-(4-(phenyldiazenyl)phenyl)benzenesulfonamide ***5f****.* Yellow oil, yield 35%; m.p. 190–192 °C; IR (KBr) 3225, 1322, 1150 cm^{-1}; ^1H NMR ($CDCl_3$) δ 3.87 (s, 3H, OCH_3), 3.93 (s, 3H, OCH_3), 5.35 (s, 2H, CH_2), 6.49–6.52 (dd, 2H, *H*arom), 6.55 (m, 1H, *H*arom), 7.34 (d, 5H, *H*arom), 7.47–7.53 (m, 4H, *H*arom), 7.78 (d, 2H, *H*arom), 7.80 (d, 2H, Harom), 7.85–7.87 (m, 2H, *H*arom), 10.25 (s, 1H, N*H*); ^{13}C NMR ($CDCl_3$) δ 50.29, 55.80, 56.19, 99.5 0, 104.64, 118.33, 120.36, 121.47, 122.86, 123.67, 126.84, 128.75, 129.08, 131.21, 133.88, 141.85, 150.60, 150.87, 152.44, 158.25, 165.52. Anal. calcd for $C_{28}H_{25}N_5O_4S$: C 63.74, H 4.78, N 13.27; Found C 63.77, H 4.76, N 13.28.

4.2. Biological assays

4.2.1. Aromatase activity inhibition assay and IC_{50} calculation

The aromatase inhibitory activity of the novel compounds was determined using a commercial fluorimetric assay (Aromatase CYP19A Inhibitor Screening kit, BioVision, Milpitas, CA, USA). The assay utilizes a fluorogenic aromatase substrate, that is converted into a highly fluorescent metabolite detected in the visible range (Ex/Em = 488/527 nm), ensuring a high signal-to-background ratio with little interference by autofluorescence.

The inhibition assay and the IC_{50} calculation were performed as reported in a previous work [37,38]. Concentration-response curves were fitted with GraphPad Prism 5.0 (GraphPad Software, San Diego, CA, USA).

4.2.2. Cell viability evaluation

4.2.2.1. Cell culture. Human skin fibroblasts (HFF-1-SCRC-1041™) and human breast cancer cells (MCF7-HTB-22 ™) were purchased from ATCC and maintained in Dulbecco's modified Eagle's medium (DMEM) high glucose (EuroClone, Milan, Italy) supplemented with 10% of fetal bovine serum (FBS) and 1% of penicillin/streptomycin (Gibco - Thermofisher Scientific, MD, USA).

4.2.2.2. Cell metabolic activity (MTT assay). Cell metabolic activity of HFF-1 and MCF7 cells was assessed by MTT (3-(4,5-Dimethylthiazol-2-yl)-2,5-Diphenyltetrazolium Bromide) test (Sigma Aldrich, Milan, Italy). Cells were seeded (0.1×10^4/well) in a 96-well tissue culture-treated plate (Falcon®, Corning Incorporated, NY, USA) and let them adhere for 24 h. Next, medium was removed, and the cell monolayer was incubated in the presence of loading concentrations of compounds **3b**, **3f** and **5f** (0–250 μM) for 24, 48 and 72 h. After the exposure time, cells were incubated with 100 μl/well of MTT (5 mg/mL) 1:10 with fresh growth medium (final concentration 0.5 mg/mL) for 4 h at 37 °C and 5% CO_2. Finally, the MTT solution was removed and replaced with 100 μl/well of DMSO. Cells were incubated for additional 20 min at 37 °C and 5% CO_2 and afterwards gently swirled for 10 min at room temperature. The optical density was measured at 540 nm by means of a spectrophotometer (Multiskan GO, Thermo Scientific, Monza, Italy). Results were expressed as the percentage of cells in the presence of vehicle (DMSO) set as 100% and each experiment was performed in triplicate (n = 3). Concentration-response curves and IC_{50} were fitted and calculated with GraphPad Prism 5.0 (GraphPad Software, San Diego, CA, USA).

4.2.2.3. Cytotoxicity test (lactate dehydrogenase release). MCF7 cells were seeded and stimulated as previously described for the MTT test. After the exposure time, cell supernatants were collected, centrifugated at 450×*g* for 4 min and stored on ice. To quantify the cytotoxicity of loading concentrations of compounds **3b**, **3f** and **5f** (0–250 μM), the CytoTox 96® Non-Radioactive Cytotoxicity Assay (Promega Corporation, WI, USA) was performed. The CytoTox 96® Assay quantitatively measures lactate dehydrogenase (LDH), a stable cytosolic enzyme that is released upon cell lysis. Released LDH in supernatants is measured with a 30-min coupled enzymatic assay, which results in the conversion of a tetrazolium salt (iodonitrotetrazolium violet; INT) into a red formazan product. The absorbance signal was measured at 490 and 690 nm (background) with a spectrophotometer (Multiskan GO, Thermo Scientific, Monza, Italy). The results were normalized on MTT absorbances and expressed as fold increases on the LDH released by cultures in the presence of vehicle (DMSO) set as 1.

4.2.2.4. Detection of apoptosis. MCF7 cells were cultured in 6-well plates for 24 h at 37 °C in a humidified atmosphere. The growth medium was then removed, and the cells were subsequently exposed to increasing concentrations of the **3f** compound. After 24 h, cells were washed once with PBS at room temperature. Next, cells were trypsinized and collected by centrifugation together with floating cells in the supernatants. Apoptotic and necrotic cells were detected after staining cells with APC Annexin-V antibody (BD Pharmingen, San Jose, CA, USA) and 7-Aminoactinomycin D (7AAD) (Thermo Fisher Scientific, MA, USA), following the manufacturer's instructions. Briefly, samples were incubated in 197 μL of binding buffer and 3 μL of APC Annexin-V for 15 min at room temperature in the dark. Volumes were afterwards doubled, cells were washed once by centrifugation and re-suspended into 300 μL of binding buffer with 7AAD. The fluorescence was determined by a CytoFlex flow cytometer (Beckman Coulter, CA, USA). Data acquisition (2×10^4 events/sample) and data analysis were performed with the CytExpert Software (Beckman Coulter, CA, USA). The percentages of viable cells (Annexin V^-; $7AAD^-$) were detected in the lower left quadrant (unstained) of density plots, as well as the cells in apoptosis (Annexin $V^+/7AAD^-$, lower right quadrant), late apoptosis (Annexin $V^+/7AAD^+$, upper right quadrant) and necrosis (Annexin $V^-/7AAD^+$, upper left quadrant).

4.2.2.5. Cell cycle analysis. The MCF7 cells were seeded and exposed as previously described for the apoptosis assay. After 72 h, the medium was removed and cells were washed once with PBS, trypsinized and collected by centrifugation. Next, the cells were fixed in cold ethanol 70% v/v and kept at 4 °C overnight. After that, the cells were gently washed with cold PBS and centrifuged at 2700×*g* for 10 min at 4 °C. After having discarded supernatants, each sample was incubated in 300 μL of the staining solution containing PBS without calcium and magnesium, RNase 100 μg/mL (stock solution 10 mg/mL in 10 mM sodium acetate buffer, pH 7.4) and PI 10 μg/mL (stock solution 1 mg/mL in water) (all purchased by Sigma Aldrich, MI, USA) and kept at 4 °C overnight in the dark. PI fluorescence was detected by a flow cytometer equipped with a 488 nm laser (CytoFlex flow cytometer, Beckman Coulter, CA, USA) in the FL-3 channel (620 nm of wavelength emission). 2×10^4 events/sample were collected and analyzed with CytExpert

Software (Beckman Coulter, CA, USA). The percentage of cells in G1, S, or G2 phase of the cell cycle was calculated after mathematical modeling of histograms using the ModFit LT™ software (Verity Software House, CA, USA).

4.2.2.6. Statistics. Data are presented as mean values ± standard deviations (S.D.) of three independent experiments. Statistical differences were determined by one-way ANOVA and *post hoc* Tukey multiple comparison tests using the Prism software (version 5.0, GraphPad Software, San Diego, CA, USA). P values < 0.05 were considered statistically significant.

4.3. Computational studies

Computational studies were carried out for compound **3f** by using X-ray solved structure of aromatase CYP19A1, whose crystal was fetched from the Protein Data Bank with entry 3EQM [48]. The protein structure was refined and optimized employing the Protein Preparation Wizard tools [49,50], available in Schrodinger Suite, allowing to add missing hydrogen atoms, correct protonation states and reconstruct incomplete side chains. Ligprep tool [51] was used to evaluate all possible tautomers and protonation states at physiological pH. The enclosing box was centered on the cognate ligand, having an edge of 15 Å × 15 Å × 15 Å and 27 Å × 27 Å × 27 Å for inner and outer boxes, respectively, and a van der Waals scaling factor equal to 0.7 was set. In order to corroborate the robustness of docking protocol, redocking analysis was performed on the cognate ligand within the aromatase binding site. Satisfactorily, the best pose of cognate ligand returned from redocking simulation showed a Root Mean Square Deviation (RMSD) value considering all heavy atoms equal to 0.756 Å. The Induced-Fit docking protocol [52–54] was employed by using GLIDE [55] with OPLS3e force field [56], in order to inspect the binding mode of the selected ligands along with conformational changes experienced by the receptor. Such structural changes are not generally observable when using standard docking protocols. Side chains prediction was performed on residues within 5 Å of the ligand poses. For the sake of completeness, induced-fit docking protocol for compounds targeting CYP19A1 aromatase was already employed elsewhere [36]. Finally, an estimation of ligand-binding affinity was obtained by running Molecular Mechanics/Generalized Born Surface Area (MM-GBSA) method implemented in Prime [54,57], which uses the VSGB 2.0 implicit solvation model [47].

In this respect, binding free energy (ΔG_{bind}) of compound 3f towards CYP19A1 was computed as reported below:

$$\Delta G_{bind} = \Delta E_{MM} + \Delta G_{solv} + \Delta G_{SA}$$

where, ΔE_{MM}, ΔG_{solv} and ΔG_{SA} correspond to minimized energy of the ligand-protein complex, solvation energy and surface area energy, respectively. For completeness and to better address molecular modeling analyses, all computational simulations were performed also for resveratrol, since it was used as reference for experimental biological evaluations.

Funding

This work was supported by FAR funds (Italian Ministry for Instruction, University and Research) assigned to Letizia Giampietro and Marialucia Gallorini. Orazio Nicolotti thanks "4FRAILTY e Sensoristica intelligente, infrastrutture e modelli gestionali per la sicurezza di soggetti fragili", codex ARS01_00345, for support.

Declaration of competing interest

The authors declare that they have no known competing financial interests or personal relationships that could have appeared to influence the work reported in this paper.

Appendix A. Supplementary data

Supplementary data to this article can be found online at https://doi.org/10.1016/j.ejmech.2021.113737.

References

[1] E.R. Simpson, M.S. Mahendroo, G.D. Means, M.W. Kilgore, M.M. Hinshelwood, S. Graham-Lorence, B. Amarneh, Y. Ito, C.R. Fisher, M.D. Michael, C.R. Mendelson, S.E. Bulun, Aromatase cytochrome P450, the enzyme responsible for estrogen biosynthesis*, Endocr. Rev. 15 (1994) 342–355, https://doi.org/10.1210/edrv-15-3-342.
[2] D. Ghosh, J. Lo, C. Egbuta, Recent progress in the discovery of next generation inhibitors of aromatase from the structure-function perspective, J. Med. Chem. 59 (2016) 5131–5148, https://doi.org/10.1021/acs.jmedchem.5b01281.
[3] R.W. Brueggemeier, J.C. Hackett, E.S. Diaz-Cruz, Aromatase inhibitors in the treatment of breast cancer, Endocr. Rev. 26 (2005) 331–345, https://doi.org/10.1210/er.2004-0015.
[4] O. Shimozawa, M. Sakaguchi, H. Ogawa, N. Harada, K. Mihara, T. Omura, Core glycosylation of cytochrome P-450(arom). Evidence for localization of N terminus of microsomal cytochrome P-450 in the lumen, J. Biol. Chem. 268 (1993) 21399–21402.
[5] T. Jha, N. Adhikari, A.K. Halder, A. Saha, Ligand- and Structure-Based Drug Design of Non-steroidal Aromatase Inhibitors (NSAIs) in Breast Cancer, 2015, pp. 400–470, https://doi.org/10.4018/978-1-4666-8136-1.ch011.
[6] H.J. Chan, K. Petrossian, S. Chen, Structural and functional characterization of aromatase, estrogen receptor, and their genes in endocrine-responsive and –resistant breast cancer cells, J. Steroid Biochem. Mol. Biol. 161 (2016) 73–83, https://doi.org/10.1016/j.jsbmb.2015.07.018.
[7] E. Amenyogbe, G. Chen, Z. Wang, X. Lu, M. Lin, A.Y. Lin, A review on sex steroid hormone estrogen receptors in mammals and fish, Internet J. Endocrinol. 2020 (2020) 5386193, https://doi.org/10.1155/2020/5386193.
[8] J. Blakemore, F. Naftolin, Aromatase: contributions to physiology and disease in women and men, Physiology 31 (2016) 258–269, https://doi.org/10.1152/physiol.00054.2015.
[9] P. Bhardwaj, C.C. Au, A. Benito-Martin, H. Ladumor, S. Oshchepkova, R. Moges, K.A. Brown, Estrogens and breast cancer: mechanisms involved in obesity-related development, growth and progression, J. Steroid Biochem. Mol. Biol. 189 (2019) 161–170, https://doi.org/10.1016/j.jsbmb.2019.03.002.
[10] N. Adhikari, S.K. Baidya, T. Jha, Effective anti-aromatase therapy to battle against estrogen-mediated breast cancer: comparative SAR/QSAR assessment on steroidal aromatase inhibitors, Eur. J. Med. Chem. 208 (2020) 112845, https://doi.org/10.1016/j.ejmech.2020.112845.
[11] A. Peters, P. Tadi, Aromatase inhibitors, in: in: Treasure Island (FL), 2021.
[12] W.C. Schwarzel, W.G. Kruggel, H.J. Brodie, Studies on the mechanism of estrogen biosynthesis. 8. The development of inhibitors of the enzyme system in human placenta, Endocrinology 92 (1973) 866–880, https://doi.org/10.1210/endo-92-3-866.
[13] R.W. Brueggemeier, E.E. Floyd, R.E. Counsell, Synthesis and biochemical evaluation of inhibitors of estrogen biosynthesis, J. Med. Chem. 21 (1978) 1007–1011, https://doi.org/10.1021/jm00208a002.
[14] S. Tenti, P. Correale, S. Cheleschi, A. Fioravanti, L. Pirtoli, Aromatase inhibitors-induced musculoskeletal disorders: current knowledge on clinical and molecular aspects, Int. J. Mol. Sci. 21 (2020), https://doi.org/10.3390/ijms21165625.
[15] The Breast International Group (BIG) 1-98 Collaborative Group, A comparison of letrozole and tamoxifen in postmenopausal women with early breast cancer, N. Engl. J. Med. 353 (2005) 2747–2757, https://doi.org/10.1056/NEJMoa052258.
[16] O.L. Tseng, J.J. Spinelli, C.C. Gotay, W.Y. Ho, M.L. McBride, M.G. Dawes, Aromatase inhibitors are associated with a higher fracture risk than tamoxifen: a systematic review and meta-analysis, Ther. Adv. Musculoskelet. Dis. 10 (2018) 71–90, https://doi.org/10.1177/1759720X18759291.
[17] F. Khosrow-Khavar, K.B. Filion, S. Al-Qurashi, N. Torabi, N. Bouganim, S. Suissa, L. Azoulay, Cardiotoxicity of aromatase inhibitors and tamoxifen in postmenopausal women with breast cancer: a systematic review and meta-analysis of randomized controlled trials, Ann. Oncol. Off. J. Eur. Soc. Med. Oncol. 28 (2017) 487–496, https://doi.org/10.1093/annonc/mdw673.
[18] B. De Filippis, A. Ammazzalorso, M. Fantacuzzi, L. Giampietro, C. Maccallini, R. Amoroso, Anticancer activity of stilbene-based derivatives, ChemMedChem 12 (2017) 558–570, https://doi.org/10.1002/cmdc.201700045.
[19] P. Pecyna, J. Wargula, M. Murias, M. Kucinska, More than resveratrol: new insights into stilbene-based compounds, Biomol 10 (2020), https://doi.org/10.3390/biom10081111.
[20] A.J. Nielsen, J. McNulty, Polyphenolic natural products and natural product-

inspired steroidal mimics as aromatase inhibitors, Med. Res. Rev. 39 (2019) 1274–1293, https://doi.org/10.1002/med.21536.
[21] T.P. Kondratyuk, E.-J. Park, L.E. Marler, S. Ahn, Y. Yuan, Y. Choi, R. Yu, R.B. van Breemen, B. Sun, J. Hoshino, M. Cushman, K.C. Jermihov, A.D. Mesecar, C.J. Grubbs, J.M. Pezzuto, Resveratrol derivatives as promising chemopreventive agents with improved potency and selectivity, Mol. Nutr. Food Res. 55 (2011) 1249–1265, https://doi.org/10.1002/mnfr.201100122.
[22] R. Ahmadi, M.A. Ebrahimzadeh, Resveratrol - a comprehensive review of recent advances in anticancer drug design and development, Eur. J. Med. Chem. 200 (2020) 112356, https://doi.org/10.1016/j.ejmech.2020.112356.
[23] B. De Filippis, L. De Lellis, R. Florio, A. Ammazzalorso, P. Amoia, M. Fantacuzzi, L. Giampietro, C. Maccallini, R. Amoroso, S. Veschi, A. Cama, Synthesis and cytotoxic effects on pancreatic cancer cellsof resveratrol analogs, Med. Chem. Res. 28 (2019) 984–991.
[24] A.J. Nielsen, S. Raez-Villanueva, D.J. Crankshaw, A.C. Holloway, J. McNulty, Synthesis of α-methylstilbenes using an aqueous Wittig methodology and application toward the development of potent human aromatase inhibitors, Bioorg. Med. Chem. Lett 29 (2019) 1395–1398, https://doi.org/10.1016/j.bmcl.2019.03.033.
[25] B. Sun, J. Hoshino, K. Jermihov, L. Marler, J.M. Pezzuto, A.D. Mesecar, M. Cushman, Design, synthesis, and biological evaluation of resveratrol analogues as aromatase and quinone reductase 2 inhibitors for chemoprevention of cancer, Bioorg. Med. Chem. 18 (2010) 5352–5366, https://doi.org/10.1016/j.bmc.2010.05.042.
[26] L.M. Lima, E.J. Barreiro, Bioisosterism: a useful strategy for molecular modification and drug design, Curr. Med. Chem. 12 (2005) 23–49, https://doi.org/10.2174/0929867053363540.
[27] X. Li, Y. Xie, H. Xie, J. Yang, D. Chen, π-π conjugation enhances oligostilbene's antioxidant capacity: evidence from α-viniferin and caraphenol A, Mol 23 (2018), https://doi.org/10.3390/molecules23030694.
[28] G. Lizard, N. Latruffe, D. Vervandier-Fasseur, Aza- and azo-stilbenes: bioisosteric analogs of resveratrol, Mol 25 (2020), https://doi.org/10.3390/molecules25030605.
[29] L. Giampietro, A. Laghezza, C. Cerchia, R. Florio, L. Recinella, F. Capone, A. Ammazzalorso, I. Bruno, B. De Filippis, M. Fantacuzzi, C. Ferrante, C. Maccallini, P. Tortorella, F. Verginelli, L. Brunetti, A. Cama, R. Amoroso, F. Loiodice, A. Lavecchia, Novel phenyldiazenyl fibrate analogues as PPAR α/γ/δ pan-agonists for the amelioration of metabolic syndrome, ACS Med. Chem. Lett. 10 (2019) 545–551, https://doi.org/10.1021/acsmedchemlett.8b00574.
[30] F.A. Khan, S. Mushtaq, S. Naz, U. Farooq, A. Zaidi, S.M. Bukhari, A. R, M.S. Mubarak*, Sulfonamides as potential bioactive scaffolds, Curr. Org. Chem. 22 (2018) 818–830, https://doi.org/10.2174/1385272822666180122153839.
[31] A. Ammazzalorso, B. De Filippis, L. Giampietro, R. Amoroso, N-acylsulfonamides, Synthetic routes and biological potential in medicinal chemistry, Chem. Biol. Drug Des. 90 (2017) 1094–1105, https://doi.org/10.1111/cbdd.13043.
[32] R. Pingaew, V. Prachayasittikul, P. Mandi, C. Nantasenamat, S. Prachayasittikul, S. Ruchirawat, V. Prachayasittikul, Synthesis and molecular docking of 1,2,3-triazole-based sulfonamides as aromatase inhibitors, Bioorg. Med. Chem. 23 (2015) 3472–3480, https://doi.org/10.1016/j.bmc.2015.04.036.
[33] M.M. Ghorab, M.S. Alsaid, G.H. Al-Ansary, G.A. Abdel-Latif, D.A. Abou El Ella, Analogue based drug design, synthesis, molecular docking and anticancer evaluation of novel chromene sulfonamide hybrids as aromatase inhibitors and apoptosis enhancers, Eur. J. Med. Chem. 124 (2016) 946–958, https://doi.org/10.1016/j.ejmech.2016.10.020.
[34] R. Pingaew, P. Mandi, V. Prachayasittikul, S. Prachayasittikul, S. Ruchirawat, V. Prachayasittikul, Synthesis, molecular docking, and QSAR study of sulfonamide-based indoles as aromatase inhibitors, Eur. J. Med. Chem. 143 (2018) 1604–1615, https://doi.org/10.1016/j.ejmech.2017.10.057.
[35] M.M. Ghorab, M.S. Alsaid, N. Samir, G.A. Abdel-Latif, A.M. Soliman, F.A. Ragab, D.A. Abou El Ella, Aromatase inhibitors and apoptotic inducers: design, synthesis, anticancer activity and molecular modeling studies of novel phenothiazine derivatives carrying sulfonamide moiety as hybrid molecules, Eur. J. Med. Chem. 134 (2017) 304–315, https://doi.org/10.1016/j.ejmech.2017.04.028.
[36] F. Caporuscio, G. Rastelli, C. Imbriano, A. Del Rio, Structure-based design of potent aromatase inhibitors by high-throughput docking, J. Med. Chem. 54 (2011) 4006–4017, https://doi.org/10.1021/jm2000689.
[37] M. Di Matteo, A. Ammazzalorso, F. Andreoli, I. Caffa, B. De Filippis, M. Fantacuzzi, L. Giampietro, C. Maccallini, A. Nencioni, M.D. Parenti, D. Soncini, A. Del Rio, R. Amoroso, Synthesis and biological characterization of 3-(imidazole-1-ylmethyl)piperidine sulfonamides as aromatase inhibitors, Bioorg. Med. Chem. Lett 26 (2016) 3192–3194, https://doi.org/10.1016/j.bmcl.2016.04.078.
[38] M. Fantacuzzi, B. De Filippis, M. Gallorini, A. Ammazzalorso, L. Giampietro, C. Maccallini, Z. Aturki, E. Donati, R.S. Ibrahim, E. Shawky, A. Cataldi, R. Amoroso, Synthesis, biological evaluation, and docking study of indole aryl sulfonamides as aromatase inhibitors, Eur. J. Med. Chem. 185 (2020) 111815, https://doi.org/10.1016/j.ejmech.2019.111815.
[39] A. Ammazzalorso, M. Gallorini, M. Fantacuzzi, N. Gambacorta, B. De Filippis, L. Giampietro, C. Maccallini, O. Nicolotti, A. Cataldi, R. Amoroso, Design, synthesis and biological evaluation of imidazole and triazole-based carbamates as novel aromatase inhibitors, Eur. J. Med. Chem. 211 (2021) 113115, https://doi.org/10.1016/j.ejmech.2020.113115.
[40] F.K. Chan, K. Moriwaki, M.J. De Rosa, Detection of necrosis by release of lactate dehydrogenase activity, Methods Mol. Biol. 979 (2013) 65–70.
[41] C. Amaral, C. Varela, M. Borges, E. Tavares da Silva, F.M.F. Roleira, G. Correia-da-Silva, N. Teixeira, Steroidal aromatase inhibitors inhibit growth of hormone-dependent breast cancer cells by inducing cell cycle arrest and apoptosis, Apoptosis 18 (11) (2013) 1426–1436.
[42] D.-X. He, X.-L. Wu, C.-X. Lu, X.-T. Gu, G.-Y. Zhang, X. Ma, D.-Q. Liu, Genome-wide analysis of the three-way interplay among gene expression, estrogen receptor expression and chemotherapeutic sensitivity in breast cancer, Oncol. Rep. 38 (2017) 3392–3402, https://doi.org/10.3892/or.2017.6033.
[43] R. Simstein, M. Burow, A. Parker, C. Weldon, B. Beckman, Apoptosis, chemoresistance, and breast cancer: insights from the MCF-7 cell model system, Exp. Biol. Med. 228 (2003) 995–1003, https://doi.org/10.1177/153537020322800903.
[44] A. Brodie, D. Jelovac, L. Macedo, G. Sabnis, S. Tilghman, O. Goloubeva, Therapeutic observations in MCF-7 aromatase xenografts, Clin. Canc. Res. 15 (11) (2005) 884s–888s.
[45] G. Augimeri, G. La Camera, L. Gelsomino, C. Giordano, S. Panza, D. Sisci, C. Morelli, B. Győrffy, D. Bonofiglio, S. Andò, I. Barone, S. Catalano, Evidence for enhanced exosome production in aromatase inhibitor-resistant breast cancer cells, Int. J. Mol. Sci. 21 (2020) 5841.
[46] S. Veschi, S. Carradori, L. De Lellis, R. Florio, D. Brocco, D. Secci, P. Guglielmi, M. Spano, A.P. Sobolev, A. Cama, Synthesis and evaluation of a large library ofnitroxoline derivatives as pancreatic cancerantiproliferative agents, J. Enzym. Inhib. Med. Chem. 35 (2020) 1331–1344.
[47] J. Li, R. Abel, K. Zhu, Y. Cao, S. Zhao, R.A. Friesner, The VSGB 2.0 model: a next generation energy model for high resolution protein structure modeling, Proteins 79 (2011) 2794–2812, https://doi.org/10.1002/prot.23106.
[48] D. Ghosh, J. Griswold, M. Erman, W. Pangborn, Structural basis for androgen specificity and oestrogen synthesis in human aromatase, Nature 457 (2009) 219–223, https://doi.org/10.1038/nature07614.
[49] Schrödinger Release 2020-4: Protein Preparation Wizard, Epik, Schrödinger, LLC, New York, NY, 2020, 2016; Impact, Schrödinger, LLC, New York, NY, 2016; Prime, Schrödinger, LLC, New York, NY, No Title, (n.d.).
[50] G.M. Sastry, M. Adzhigirey, T. Day, R. Annabhimoju, W. Sherman, Protein and ligand preparation: parameters, protocols, and influence on virtual screening enrichments, J. Comput. Aided Mol. Des. 27 (2013) 221–234, https://doi.org/10.1007/s10822-013-9644-8.
[51] Schrödinger Release 2020-4, LigPrep, Schrödinger, LLC, New York, NY, No Title, 2020 (n.d.).
[52] Schrödinger Release 2020-4: Induced Fit Docking Protocol; Glide, Schrödinger, LLC, New York, NY, 2020, 2016; Prime, Schrödinger, LLC, New York, NY, No Title, (n.d.).
[53] W. Sherman, T. Day, M.P. Jacobson, R.A. Friesner, R. Farid, Novel procedure for modeling ligand/receptor induced fit effects, J. Med. Chem. 49 (2006) 534–553, https://doi.org/10.1021/jm050540c.
[54] Schrödinger Release 2020-4: Prime, Schrödinger, LLC, New York, NY, No Title, 2020 (n.d.).
[55] R.A. Friesner, J.L. Banks, R.B. Murphy, T.A. Halgren, J.J. Klicic, D.T. Mainz, M.P. Repasky, E.H. Knoll, M. Shelley, J.K. Perry, D.E. Shaw, P. Francis, P.S. Shenkin, Glide: a new approach for rapid, accurate docking and scoring. 1. Method and assessment of docking accuracy, J. Med. Chem. 47 (2004) 1739–1749, https://doi.org/10.1021/jm0306430.
[56] E. Harder, W. Damm, J. Maple, C. Wu, M. Reboul, J.Y. Xiang, L. Wang, D. Lupyan, M.K. Dahlgren, J.L. Knight, J.W. Kaus, D.S. Cerutti, G. Krilov, W.L. Jorgensen, R. Abel, R.A. Friesner, OPLS3: a force field providing broad coverage of drug-like small molecules and proteins, J. Chem. Theor. Comput. 12 (2016) 281–296, https://doi.org/10.1021/acs.jctc.5b00864.
[57] S. Genheden, U. Ryde, The MM/PBSA and MM/GBSA methods to estimate ligand-binding affinities, Expet Opin. Drug Discov. 10 (2015) 449–461, https://doi.org/10.1517/17460441.2015.1032936.